

AERODYNAMIC DESIGN OPTIMISATION FOR A HELICOPTER CONFIGURATION INCLUDING A ROTATING ROTOR HEAD

Christian Breitsamter, Moritz Grawunder, Roman Reß
Institute of Aerodynamics and Fluid Mechanics, Technische Universität München

Christian.Breitsamter@aer.mw.tum.de

Keywords: *Helicopter, Drag reduction, Bluff body wake, Flow control, Wind tunnel testing*

Abstract

Aerodynamic drag is an important consideration in helicopter design to decrease fuel consumption and associated emissions. The project ‘Aerodynamic Design Optimisation of a Helicopter Fuselage Including a Rotating Rotor Head’ – ADHeRo –, within the frame of the European Community’s Clean Sky Green Rotorcraft Consortium, aims to reduce parasite drag of twin engine light class utility helicopters. Performing comprehensive wind tunnel tests and numerical simulations, aerodynamic forces and moments, surface pressure distributions and wake flow fields are analyzed in detail for a specific baseline configuration. Shape modifications and means of passive flow control are applied to diminish flow separation and wake flow regions associated with high pressure drag. Consequently, two modified skid landing gears have been designed, namely a retrofit variant and a more progressive one. These modified skid landing gears provide an overall reduction in drag of 20.9% and 23.1%, respectively. In addition, solutions focusing on both vortex generators located at the fuselage belly ahead of the back door and port and starboard strake elements along the back door results in further drag reduction of 1.4%. Therefore, an overall drag saving of 22.3% is possible by adding retrofit parts designed within ADHeRo. The technology readiness level suggests that the corresponding configurations could be commercialised within a few years. Thus, ADHeRo is making an important contribution to reduce the environmental impact of light weight utility helicopters along with lowering operational costs through reduced fuel consumption.

1 Introduction

Twin-engine light (TEL) class helicopters are ideal for critical missions, including helicopter emergency medical services, search and rescue, and law enforcement activities. With a focus on novel designs that reduce emissions in air transport, the Green Rotorcraft Consortium (GRC) of the European Community’s Clean Sky programme is addressing environmental issues in the rotorcraft domain [1]. Regarding the helicopter fleet of the year 2000, 10% of the global flight hours are attributed to TEL class civil helicopters. Due to the increasing number of missions it is strongly desirable to enhance the efficiency of this class of helicopters. The power requirements in fast level flight results approximately to 55 % from parasite drag, to 40% from the main rotor and to 5 % from the tail rotor [2], [3].

Aiming on parasite drag constitutes an important approach for obtaining a more efficient helicopter design. Parasite drag, evoked here mainly by pressure drag, is generally reduced by optimising an aircraft’s shape [4], [5]. However, the shape is subject to other, often conflicting, constraints, as the design process of utility helicopters is driven by their broad range of operations and applications [6], [7]. In consequence, it is mostly not possible to choose an aerodynamic ‘optimal’ shape, since aerodynamic design solutions have to account for these operational constraints [8]. A typical conflict arises in the aft body region where the specifications often require a rear loading capability. Therefore, it is not feasible to minimize parasite drag in the aft body region by streamlined surfaces [9].

In this context, the project ‘Aerodynamic Design Optimisation of a Helicopter Fuselage Including a Rotating Rotor Head’ – ADHeRo – (<http://www.adhero.de>), aims on parasite drag reduction of TEL-class utility helicopters in forward flight. In parallel, the drag reduction solutions should not result in an increased fuselage down force. The main scope of the work is to develop and evaluate several drag saving design modifications with respect to a given baseline TEL configuration, cf. Refs. 10 and 11.

For ADHeRo, a specific wind tunnel model is designed, manufactured and instrumented in order to perform detailed drag measurements. The model provides high modularity to account for design modifications. The model rotor head enables the full kinematic complexity of the original design. This includes the rotation of the rotor head and the collective and cyclic pitch motion of the rotor blades to provide associated drag and lift data.

Experimental and numerical flow simulations on the baseline and modified configurations are addressed. The investigations on the baseline configuration provide the reference data for all subsequent design modifications. These modifications focus on the skid landing gear, the fuselage back door area, the mast fairing and rotor head because the corresponding flow separation and wake flow account for nearly 70% - 75% of the total parasite drag [2]. Referring to the Bo105, about 38% of parasite drag is attributed to the fuselage, 23% to the rotor head and 13% to the landing skids. These numbers clearly demonstrate the strong need for drag reduction on TEL class utility helicopters resulting in increased efficiency.

The aim of the ADHeRo project is an overall reduction in parasite drag of up to 20%. Consequently, the power requirements for light class utility helicopters could be reduced by some 10% resulting in a reduction in fuel consumption of similar magnitude. Considering the technical readiness level of the planned modifications (TRL 6, i.e. pre-production entry level) the prospective means could enter market in short time after completion of the project. Thus, ADHeRo could help reducing the environmental impact of services provided by light class utility helicopters in the near future.

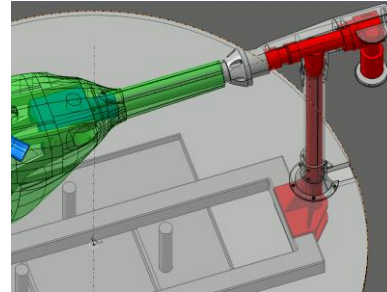
2 Geometry and Configurations

2.1 Wind Tunnel Model Geometry

The experiments are performed on a 1:5 scale detailed model of a characteristic state-of-the-art TEL utility helicopter with a maximum take-off weight of 2.95 tons (Fig. 1). Major parts of the baseline model include front and main cabin section, back door section, upper cowling, mast fairing, 5-bladed rotor head, skid landing gear and truncated tail boom. The model fuselage parts are made of composite material and connected to an inner load bearing frame made of aluminium. A tail sting element located inside the tail boom is used to attach the model frame to the model support (Fig. 1).



a) Wind tunnel model



b) Model support

Fig. 1. Baseline configuration of the ADHeRo wind tunnel model and model support.

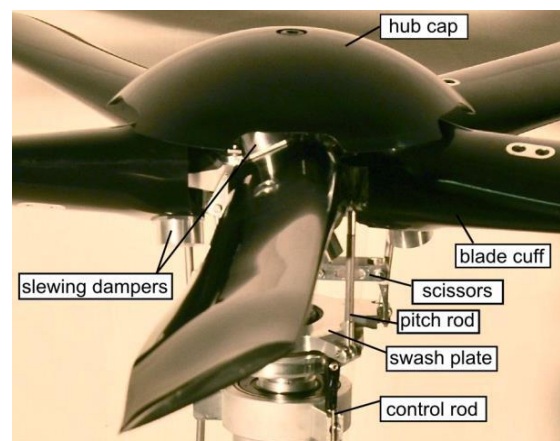


Fig. 2. Model rotor head components.

The model rotor head reproduces the full scale geometry with respect to all relevant components exposed to the flow (Fig. 2). The rotor head allows for collective and cyclic pitch motion of the blade cuffs using a fully functional swash plate. The blade cuffs are truncated at the radial position of the first effective aerodynamic blade section. The attitude of the swash blade corresponds to trimmed level flight of the full scale configuration. A detailed description of the design methodology of model and rotor head is given in Ref. 10.

2.2 Configurations

2.2.1 Baseline

A variety of configurations are investigated applying both wind tunnel tests and computational fluid dynamics to analyze the drag contribution of the main fuselage and rotor head components. The configurations associated with the baseline or reference model, respectively, comprise [10]:

- Isolated fuselage configuration
- Fuselage with skid landing gear
- Fuselage with rotor head
- Fuselage with skid landing gear and rotor head

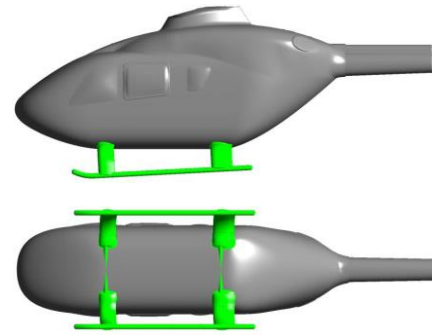
Design modifications are carried out for the skid landing gear, the back door area and the rotor head and mast fairing. In the present paper, the drag savings due to the modified shape of the landing gear and the passive flow control devices at the back door section are discussed while rotor head and mast fairing variants are still under investigation.

2.2.2 Landing Gear Shape Modifications

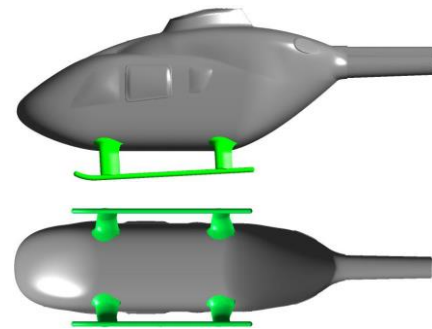
Focusing on shape optimisation, the following modifications are tested for the skid landing gear:

- Retrofit variant (L1)
- Progressive variant (L2)

The design process for the optimized landing gear variants is described in detail in Ref. 11. The form and interference drag is reduced by fairing the circular cross beams and attaching



a) Faired skid landing gear L1 (retrofit variant)



b) Faired skid landing gear L2 (progressive variant)

Fig. 3. Configurations with modified skid landings gears.

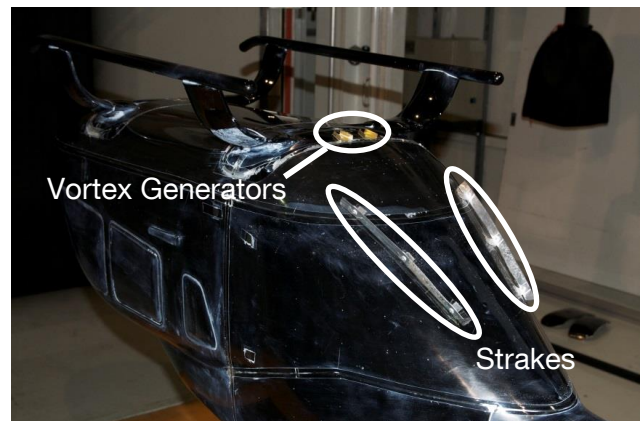


Fig. 4. Configuration with straight strakes (S1) and two pairs of vortex generators.

elements with streamlined panels (Fig. 3). The airfoil geometry DU-06-W200 (maximum thickness of 19.8% at 31.1% chord and a maximum camber of 0.5% at 84.6% chord) is used to cover the front and rear landing gear cross beams. The shape of the fairing is obtained by

extruding the airfoil geometry at its thickness maximum along the centerline of the cross beams. The thickness of the airfoil section is scaled such that it encloses the cross beam diameter with sufficient offset to the tube. This offset is necessary to comply with crash worthiness constraints. The twist at the junction between the fairing and the skids is set approximately to 0° . The twist is varied to a positive value towards the junction of the fairing with the fuselage. The impact on the static stability in pitch of the baseline fuselage is minimized by using a fairing with a larger chord at the rear relative to the front cross tube.

A more progressive design is associated with the second modification of the skid landing gear L2, which is not retrofittable to current production models. The reason is the displacement of the cross beam position vertically into the fuselage which requires structural changes on the fuselage. Because of the integrated cross beams the flow on the fuselage belly is no longer disturbed by the central cross beam elements or fairings. Thus, flow separation at the rear fuselage upsweep is delayed resulting in the desired drag savings. In addition, the integrated cross beams give a smaller frontal area leading to some further drag reduction. Compared to variant L1, the outer cross beam fairing is subject to additional shape optimizations varying chord and twist distributions of the airfoil section along the cross tube.

2.2.3 Aft Body Flow Control Devices

Also, passive flow control elements are tested to diminish the large portion of separated flow in the back door area providing further drag reduction. The flow control elements include:

- Straight strakes (retrofit variant) (S1)
- Contoured strakes (S2)
- Vortex generators (VGs)

The strakes are aimed to increase the portion of attached flow in the back door side region by alleviating the adverse pressure gradient. These elements are placed symmetrically inboard of the strong surface curvature from fuselage side edges to back door (Fig. 4). The straight strakes (S1) are designed as plate elements of constant height attached perpendicularly to the back door

surface. Therefore, these strakes can be added to an existing geometry as a retrofit variant. Regarding the optimal drag saving potential in fast forward flight, the final position, length and height of the straight strake elements are derived from wind tunnel tests (cf. Sec. 5) performing a systematic parameter variation.

The contoured strakes (S2) are the result of an automated shape optimization procedure conducted by the German Aerospace Center (DLR) and Airbus Helicopters [12]. The methodology is based on a gradient decent approach where the optimization engine is coupled with the DLR's fluid dynamics solver TAU to calculate the aerodynamics objective function and with the TAU mesh deformation module to change and adapt the surface contour geometry. The gradients are computed by means of TAU's adjoint solver to minimize the number of functional evaluations.

The vortex generators (VGs) are aimed to create pairs of counter rotating small scale streamwise vortices. Progressing downstream the vortices feed energy to the boundary layer to keep the flow attached over a larger portion of the back door upsweep area. The design of the vortex generators is based on numerical flow simulations for the baseline configuration. One primary design parameter is the boundary layer thickness δ , predicted through these simulations, giving an estimation for the height of the VGs. An appropriate VG length is approximately 3.5δ and the inclination relative to the incoming flow is set to ± 15 deg. Considering the spacing between neighboring pairs of vortex generators [13], a maximum of 5 vortex generator pairs can be placed in the region of interest. The optimal positioning and number of these pairs of vortex generators is again determined by wind tunnel tests.

3 Wind Tunnel Experiments

3.1 Facility and Test Conditions

The wind tunnel investigations have been carried out in the large low speed facility A of the Institute of Aerodynamics and Fluid Mechanics (AER) of the Technische Universität München (TUM). This closed return wind tunnel can be operated with both open and closed test sections

at maximum usable velocities of 75 *m/s* and 65 *m/s*, respectively. Test section dimensions are 1.8 *m* in height, 2.4 *m* in width and 4.8 *m* in length. The test section flow was carefully inspected and calibrated documenting a turbulence level less than 0.4%, an uncertainty in the free stream direction of less than 0.2 deg, and a variation of static pressure normalized by dynamic pressure of less than 0.4% along the relevant test section part. Uncertainties in the spatial and temporal mean velocity distributions are less than 0.067%. Because tests are also conducted for larger angles of attack and sideslip the open test section is used.

The ADHeRo measurements have been made at a free stream reference velocity of $U_\infty = 40$ *m/s* at ambient pressure p_∞ and ambient temperature T_∞ . The corresponding Reynolds number is $Re \approx 1 \times 10^6$ and the free stream Mach number is $Ma_\infty \approx 0.1$. Results are mainly shown for an angle of attack of $\alpha = 0^\circ$ and an angle of sideslip of $\beta = 0^\circ$. For some cases, an angle-of-attack range of $-10^\circ \leq \alpha \leq +10^\circ$ at $\beta = 0^\circ$ is considered.

3.2 Model Integration

The model is sting mounted via the tail sting located inside the tail boom model part. The model tail sting is connected to a specific model support (Fig. 1). This support provides minimum model interference compared to standard solutions using belly or head stings. The load bearing support structure is covered so that only the aerodynamic loads acting on the model are measured. The model can be rolled by the support rolling unit and yawed by the turntable unit of the under-floor balance. Both units are driven by gears and stepper motors. The angle of attack and the angle of sideslip of the model are then set by an appropriate combination of yaw and roll angles derived from a transfer matrix.

3.3 Measurement Techniques

Here, results are shown for aerodynamic forces and moments and wake flow fields.

3.3.1 Aerodynamic Loads

The overall forces and moments are measured using an external six-component under-floor balance. The accuracy based on maximum loads

is 0.025% for the force and moment components. These load measurements are undertaken for the baseline and associated partial configurations (i.e. with and without landing gear, rotor head, etc.) as well as for all design modifications (here: L1, L2, S1, S2, VGs and combinations). An internal six-component strain gauge balance is used to obtain the forces and moments acting on specific configuration components such as the landing gear and the (rotating) rotor head. The accuracy of the internal balance based on maximum loads ranges from 0.05% to 0.1% for the force components and from 0.8% to 1.2% for the moment components. Thus, interference loads can be obtained focusing here especially on interference drag. Combining the loads for complete and partial configurations as well as for components a detailed drag breakdown is possible, i.e. the drag contribution of the fuselage, skid landing gear, and rotor head as well as the interference drag of skid landing gear on fuselage and rotor head on fuselage can be quantified.

3.3.2 Flow Fields

Cross flow velocity fields are obtained applying Stereo Particle Image Velocimetry (Stereo PIV). The main system components consist of a 400 mJ double cavity Nd:YAG laser (wave length of 532 nm; maximum double pulse frequency of 10 Hz), two charge coupled device (CCD) cameras (resolution 1600 x 1186 pixels) with lenses and Scheimpflug adapter, a timer box and PIV processor for laser and camera synchronization and external triggering, an adjustable laser beam guiding arm with light sheet optics, a three axis traverse system and a particle generator. The measurement set up is shown in Fig. 5.

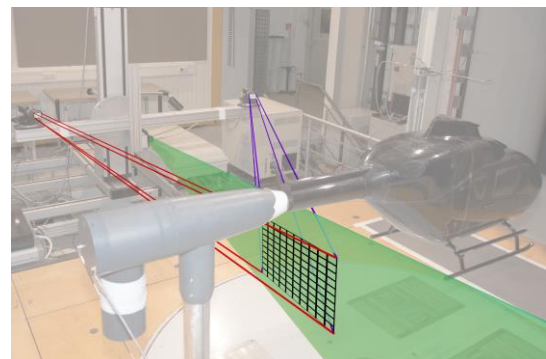


Fig. 5. Set up for Stereo PIV measurements.

The light sheet thickness is set approximately to 5 mm and the pulse delay is set to 12 μ s. Typically, velocity fields are averaged for 100 data samples. Accuracy in the mean velocity components is about 3% based on statistical analysis. Considering the measured cross flow planes, the spatial resolution based on the helicopter fuselage width is about 0.032 in the lateral and vertical direction.

4 Numerical Method

Complementary numerical simulations are performed for selected configurations. Flow modelling is based on the incompressible (Unsteady) Reynolds Averaged Navier-Stokes ((U)RANS) equations employing the commercial flow solver ANSYS CFX5 [14].

The mesh generation is carried out with the meshing tool ANSYS ICEM CFD. The computational domain is depicted in Fig. 6. It consists of an outer box with farfield dimensions of 10 times the reference length in streamwise direction $l_{x,ref}$. An inner domain is used for the rotor head to apply the sliding mesh technique for the rotor head rotation and dynamic mesh movement for the cyclic pitch [15]. Unstructured meshes are employed using the Octree method first to obtain the surface grids. Several smoothing loops are attributed to the surface grids before the volume mesh is set up with the Delaunay algorithm. The obtained volume mesh is smoothed again before adding the prism layers. The prism layers, consisting of 24 single layers, are generated near the solid walls. The equivalent dimensionless wall distance y^+ is confined below one on all no-slip surfaces. Fig. 7 presents a typical mesh for the baseline configuration. For the wake region, the grid is refined to ensure a sufficient spatial resolution for the wake vortical structures progressing downstream.

The computations are carried out employing the standard Shear Stress Transport (SST) turbulence model. For the spatial discretization, a High Resolution Scheme is employed, blending between first and second-order accuracy. The temporal discretization is realized through the application of the implicit Backward-Euler-Method with second-order accuracy. All simulations are carried out using a physical timescale

of 1×10^{-4} s. The boundary conditions for the simulations are defined by the inflow with a constant velocity profile at the inlet (turbulence intensity of 5%), the outflow with zero pressure gradient at the outlet, no-slip walls at the surface of the model and free-slip walls at the side-walls, the top and the bottom of the domain.

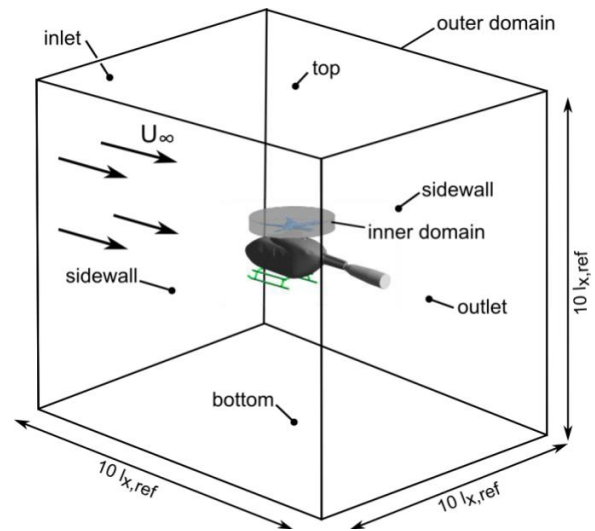


Fig. 6. Computational domain.

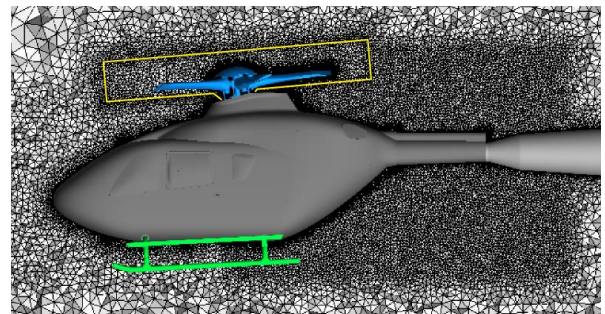


Fig. 7. Unstructured mesh for baseline configuration (rotor head domain interface indicated by yellow box).

5 Results and Analysis

The results presented combine the data obtained by experimental and numerical simulations to analyze the surface and wake flow characteristics. The change in the flow topology aimed to reduce drag by shape modification is documented by the results comparing baseline and modified skid landing gears. The influence of flow control devices is demonstrated for the aft body flow.

5.1 Skid Landing Gear

As outlined in Sec. 2.2.2, two modified skid landing gears (L1 and L2) are investigated to alleviate the amount of flow separation at the

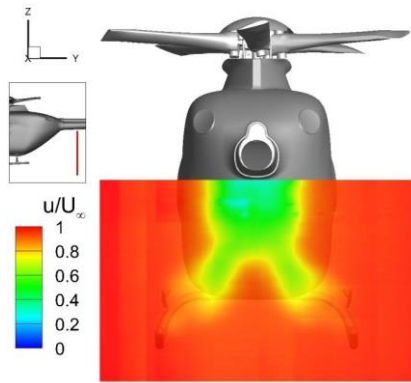
cross beams as well as to avoid the negative impact on the flow separation at the back door section.

The axial velocity fields (u/U_∞) and the corresponding fields of the root mean square (rms) velocities (u_{rms}/U_∞), taken from the Stereo PIV measurements, are analyzed for a cross flow plane in the fuselage wake. The velocity data are normalized with the freestream velocity U_∞ . Figs. 8 and 9 include the results for the baseline configuration and the configuration with the skid landing gear variant L1. For the baseline configuration, the deficit in mean axial velocity due to the flow separation at the back door upsweep region is clearly visible in the center area (Fig. 8a). There, the mean axial velocity is decreased over a wide spatial range by at least 40% to 50%. Vertical streaks of significant axial velocity deficit also indicate the wake of the vertical bars of the baseline skid landing gear featuring cylindrical cross sections. The associated rms velocity fields show two areas of increased turbulence intensities downstream of the outboard aft body region and landing gear attachments. These areas of high velocity fluctuations emanate from the massive flow separation taking place after the strong surface curvature which evokes a high adverse pressure gradient. The large areas of decreased axial velocity result in a high form and interference drag of the baseline skid landing gear configuration.

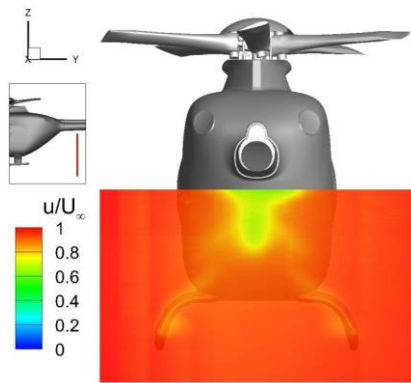
For the configurations with the faired skid landing gears (L1, L2), the areas of retarded axial flow are strongly reduced, both in their spatial expansion and in their maximum deficit levels compared to the baseline case (cf. Ref. 11). Fig. 8b includes the results for the variant L1. The aerodynamic efficiency of the applied fairings becomes obvious by two features in the contour plot of the axial velocity distribution. First, the velocity deficit associated with the wake of the faired skid landing gears is nearly not detectable. For the baseline landing gear, this wake shows a velocity deficit of approximately 40% while for the faired gears a thin sheet of velocity deficits of only 10 % is present. Second, the disturbance of the belly surface flow evoked by the rear cross beam is almost suppressed. Therefore, the flow stays attached around the aft body upsweep area over

a longer distance compared to the baseline case. Consequently, flow separation is alleviated and the velocity deficit in the wake downstream of the back door region becomes significantly reduced. Fig. 9b substantiates the lessening of the drag producing flow region as the area of increased turbulence intensities is also markedly smaller. It substantiates that fairing the attachment elements of the landing gear reduces also the interference drag on the fuselage. On the other hand, the delayed separation on the back door in the presence of the faired landing gears provides some additional downforce.

The flow field analysis is supported by the results of the URANS-SST simulations. Fig. 10 presents the surface pressure distribution (pressure coefficient c_p) and superimposed surface streamlines and Fig. 11 the normalized axial vorticity fields ($\omega_x l_{x,ref} / U_\infty$) for several cross flow planes downstream of the landing gear. For the baseline configuration, the separating shear layers in the aft body outboard regions do not roll up into a concentrated upsweep vortex along each side. Instead, vortex pairs are formed in the lower and upper aft body area indicated by the converging streamlines at the side edge regions (Fig. 10a). The downstream propagation and merging of these vortices can be taken from Fig. 11a. In contrast, the aft body streamline pattern of the configuration with the retrofittable faired skid landing gear indicates the evolution of a strong upsweep vortex (Fig. 10b). The associated separation line extends nearly over the complete side edge area. Hence, the flow topology in the aft body region is changed from an eddy type wake flow for the baseline case to a wake flow dominated by a pronounced upsweep vortex pair. The downstream development is depicted in Fig. 11b. The surface pressure distribution substantiates the positive effect of the faired skid landing gear on interference drag. By attaching the faired skid landing gear on the fuselage with a smoothed cabin bottom the back door region of increased pressure is significantly enlarged (Fig. 10b). For the baseline case, the recirculation zone extends almost over the entire back door region while for the faired skid landing gear configuration, the recirculation zone is confined to a much smaller back door area at the lower central part.

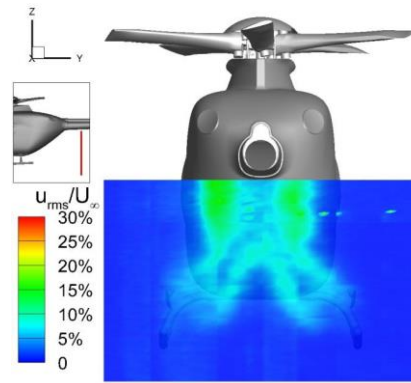


a) Baseline configuration

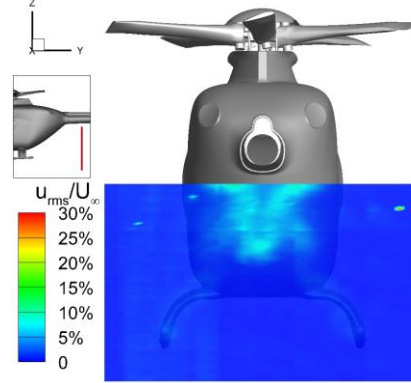


b) Configuration with faired skid landing gear L1

Fig. 8. Mean axial velocity distribution (u/U_∞) based on Stereo PIV; $Re = 1 \times 10^6$, $Ma_\infty = 0.116$, $\alpha = 0^\circ$, $\beta = 0^\circ$.

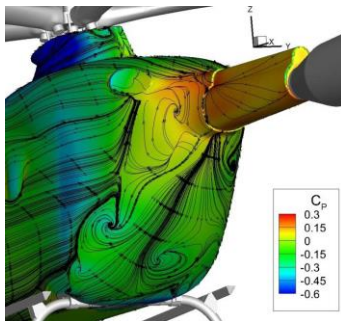


a) Baseline configuration

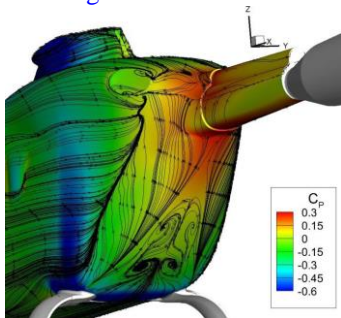


b) Configuration with faired skid landing gear L1

Fig. 9. RMS axial velocity distribution (u_{rms}/U_∞) based on Stereo PIV; $Re = 1 \times 10^6$, $Ma_\infty = 0.116$, $\alpha = 0^\circ$, $\beta = 0^\circ$.

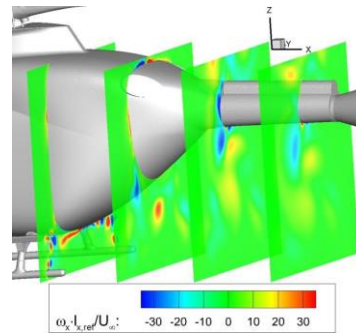


a) Baseline configuration

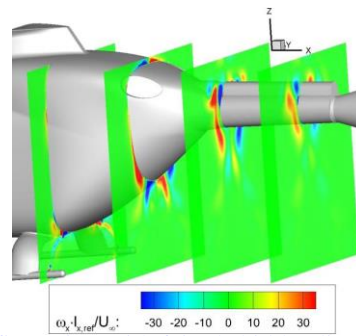


b) Configuration with faired skid landing gear L1

Fig. 10. Pressure coefficient distribution on rear fuselage and back door region and surface streamlines based on URANS-SST; $Re = 1 \times 10^6$, $Ma_\infty = 0.116$, $\alpha = 0^\circ$, $\beta = 0^\circ$.



a) Baseline configuration



b) Configuration with faired skid landing gear L1

Fig. 11. Non-dimensional axial vorticity distribution ($\omega_x l_{x,ref}/U_\infty$) based on URANS-SST; $Re = 1 \times 10^6$, $Ma_\infty = 0.116$, $\alpha = 0^\circ$, $\beta = 0^\circ$.

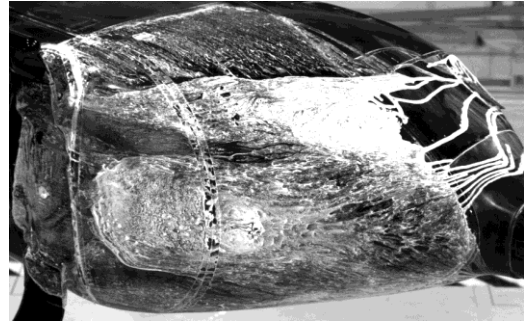
5.2 Aft Body Strakes and Vortex Generators

The back door strakes and fuselage belly vortex generators are aimed to increase the portion of attached flow in the aft body regions featuring strong surface curvature, i.e. the side edge and upsweep regions.

A surface flow visualization performed for the configuration with the faired skid landing gear L1 clearly indicates the upsweep vortex evolution along the aft body side edges and the separation zone in the aft body upper central part (Fig. 12a). This flow pattern is used to start with a systematic variation of the position, extension and height of the straight strakes (S1) and the position and number of the vortex generators (VGs). Eight positions, two heights and two design variants have been tested for the straight strake solution. For the VGs, the surface flow pattern has been examined for two stream-wise positions, two VG heights and a number of two to four VG pairs. Fig. 12b depicts the strong impact on the aft body flow for a combination of the straight strakes and two VG pairs. This combination results in the largest drag saving with respect to retrofit passive flow control for the back door flow. In comparison to the configuration with the faired skid landing gear L1, the areas of attached flow are markedly enlarged in the side edge and central aft body regions. The related drag polar and wake velocity fields are shown in Fig. 13 comparing the configurations without and with aft body flow control. The latter leads to a drag saving of about 5% (without stabilizer tail section) relative to the configuration L1. This drag saving can be nearly obtained for the angle of attack range of -10° to $+10^\circ$ (Fig. 13a). The flow control effect is also revealed by a further reduction of the area of the mean axial velocity deficit located in upper central back door section.

5.3 Drag Breakdown

As a synthesis, Fig. 14 includes drag breakdown charts for the considered configurations, namely the baseline configuration, the configuration with the faired skid landing gear L1, and configuration L1 adding the back door straight strakes (S1) and the two fuselage belly vortex generators.



a) Faired skid landing gear configuration L1



b) Faired skid landing gear configuration L1 with straight strakes and vortex generators

Fig. 12. Surface flow visualization analyzing the impact of the aft body passive flow control devices.

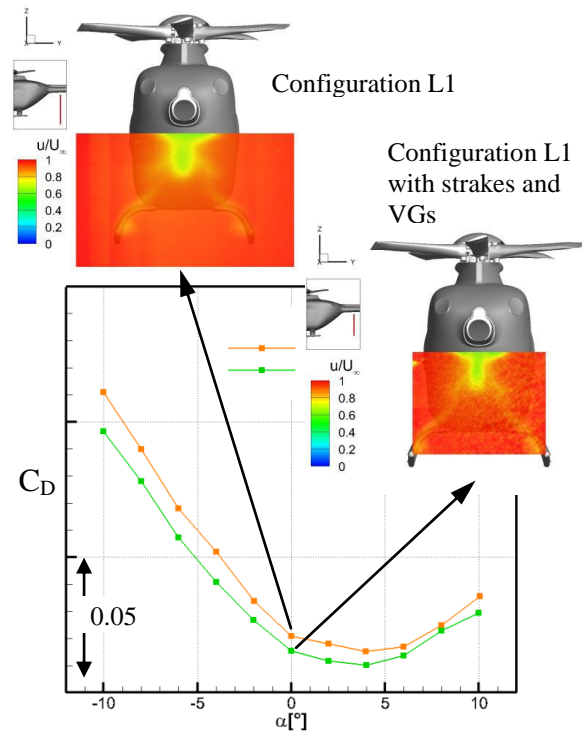
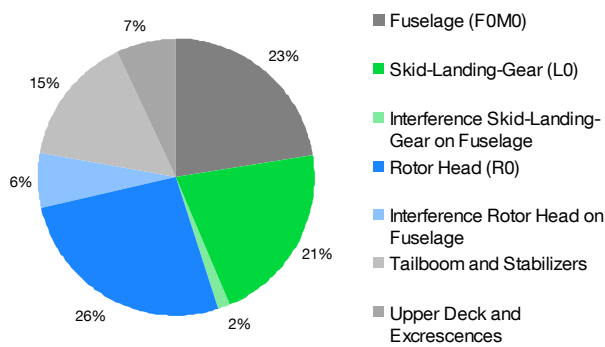


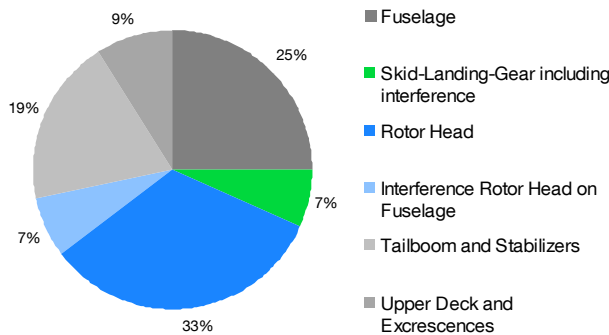
Fig. 13. Drag polar and mean axial velocity fields for the skid landing gear configuration L1 and L1 with strakes and VGs; Stereo PIV, $Re = 1 \times 10^6$, $Ma_\infty = 0.116$.

The drag breakdown charts include also the contributions which can not be measured for the wind tunnel configuration, i.e. the proportion of the complete tailboom and stabilizers and upper deck and excrescences. Those contributions are derived from numerical simulations.

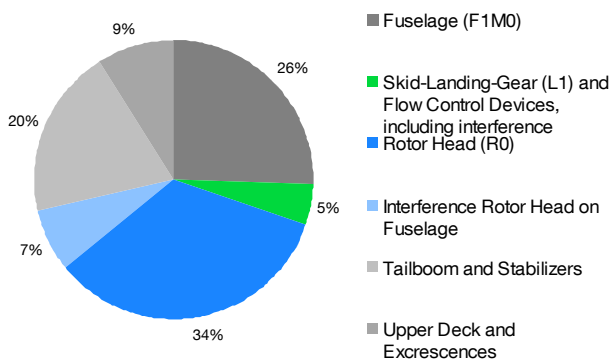
For the baseline configuration (Fig. 14a), the main drag contributions are attributed to the fuselage (23%), to the the skid landing gear (21%), and to the rotor head (26%). Such data substantiates again the motivation of the ADHeRo project to investigate drag reduction



a) Baseline configuration



a) Faired skid landing gear configuration L1



a) Configuration L1 with strakes and VGs

Fig. 14. Drag breakdown chart; $Re = 1 \times 10^6$, $Ma_\infty = 0.116$, $\alpha = 0^\circ$, $\beta = 0^\circ$.

means for these helicopter components. The contribution of the skid landing gear interference drag on the fuselage is 2% and of the rotor head on the fuselage is 6%. The drag proportions of tailboom, stabilizers, upper deck and excrescences result in 22%.

Regarding the modified skid landing gears L1 and L2, a drag reduction of 26.8% and 29.8% can be obtained for the wind tunnel configuration (no stabilizer section). Taking into account the complete helicopter configuration the drag savings are 20.9% and 23.1%, respectively. The applied fairings in combination with the smoothed cabin bottom prove highly effective for reducing parasite drag. The modified configuration with the progressive landing gear design variant L2 provides a slightly better drag reduction potential. However, the difference to the configuration with the retrofittable variant L1 is only about 3%. The drag breakdown for the configuration L1 reveals that the drag contribution of the faired skid landing gear is now markedly reduced to 7% including interference. Consequently, the contributions of fuselage and rotor head rise to 25% and 33%.

Adding the straight strakes and vortex generators provide a further drag saving of about 5% for the wind tunnel model configuration corresponding to about 1.5% for the complete helicopter configuration. Thus, the drag breakdown chart indicates that the drag contribution attributed to the faired skid landing gear together with strakes and vortex generators decreases to 5% including interference.

6 Conclusions and Outlook

In the framework of the Clean Sky Joint Technology Initiative, the Green Rotorcraft Consortium subproject ADHeRo ‘Aerodynamic Design Optimisation of a Helicopter Fuselage including a Rotating Rotor Head’ (ADHeRo) has been established to improve the aerodynamic efficiency of twin engine light class utility helicopters focusing mainly on drag reduction means. This paper presents results for skid landing gear modifications and aft body flow control devices. The data are based on wind tunnel experiments and complementary fluid dynamics simulations which confirm the drag reduction potentials for

faired skid landing gears and manipulation of the back door flow. In comparison to the reference configuration, considerable drag savings have been achieved, namely 20.9% and 23.1%, respectively, due to the faired skid landing gears which include a retrofit and a progressive variant, and 1.4% due to the aft body strakes and two pairs of vortex generators. The latter are located at the fuselage belly ahead of the strong back door upsweep. Thus the investigated configurations exceed the expected drag benefits with 22.3% in the aggregate for the retrofit solutions. The technology readiness level of the configuration modifications is that the proposed configuration modifications could be realized shortly after the end of the project. Thus, ADHeRo is making an important contribution to the reduction of the environmental impact of light weight utility helicopters. The added benefit of reduced operational costs through reduced fuel consumption will help to fasten the process of applying the drag reduction means.

Acknowledgements

The research project ADHeRo is funded within the European Community's Seventh Framework Program (FP/2007-2013) for the Clean Sky Joint Technology Initiative under grant agreement number 270563.

The authors would like to thank project partner AIRBUS Helicopters Deutschland GmbH for the fruitful collaboration and valuable support. Further, special thanks are addressed to ANSYS® for providing the flow simulation software.

References

- [1] Clean Sky JTI, Green Rotorcraft; <http://www.cleansky.eu>
- [2] Stroub R H and Rabbott J P Jr. Wasted Fuel – Another Reason for Drag Reduction, *31st Annual National Forum of the American Helicopter Society*, Washington, D.C., May 1975.
- [3] Wagner, S N. Problems of Estimating the Drag of a Helicopter, *AGARD Conference Proceedings No. 124*, April, 1973.
- [4] Leishman, J G. *Principles of Helicopter Aerodynamics*, 2nd Edition, Cambridge University Press, 2006.

- [5] Keys, C N, Wiesner, R. Guidelines for Reducing Helicopter Parasite Drag. *Journal of the American Helicopter Society*, Vol.20, Issue 31, 1975.
- [6] Kneisch, T, Krauss, R, D'Alascio, A, and Schimke, D. Optimised Rotor Head Design for an Economic Helicopter. *Proc. 37th European Rotorcraft Forum*, Gallarate, Italy, 2011.
- [7] Le Chuiton, F, Kneisch, T, Schneider, S, and Krämer, Ph. Industrial validation of numerical aerodynamics about rotor heads: towards a design optimisation at Eurocopter", *Proc. 35th European Rotorcraft Forum*, Hamburg, Germany, September 22 - 25, 2009.
- [8] Seddon, J, Newman, S. *Basic Helicopter Aerodynamics*, 2nd Edition, Blackwell Science, 2002.
- [9] Vogel, F, Breitsamter, C, and Adams, N A. Aerodynamic Analysis of a Helicopter Fuselage. *New Results in Numerical and Experimental Fluid Mechanics VII, NNFM*, Vol. 112, 2010, pp. 603-610.
- [10] Grawunder, M, Reiß, R, Breitsamter, C, and Adams, N A. Flow Characteristics of a Helicopter Fuselage Configuration Including a Rotating Rotor Head. In: *ICAS Proc., 28th Congress of the International Council of the Aeronautical Sciences, ICAS-2012-2.7.3*, Brisbane, Australia, Sept. 23-28, 2012, pp. 273.1– 273.14.
- [11] Grawunder, M, Reiß, R, and Breitsamter, C. Optimized Skid-Landing-Gears For Twin-Engine-Light Utility Helicopter. *Proc. 39th European Rotorcraft Forum, ERF-2013-093*, Moscow, Russia, Sept. 3-6, 2013, pp. 093.1– 093.14.
- [12] Zhang, Q, Garavello, A, D'Alascio, A, Schimke, D. Advanced CFD-based Optimization Methods Applied to the Industrial Design Process of Airframe Components at Airbus Helicopters, *Proc. AHS 70th Annual Forum*, Montréal, Québec, Canada, May 20– 22, 2014, pp. 1-13.
- [13] Gad-el-Hak, M. *Flow Control – Passive, Active, and Reactive Flow Management*, Cambridge University Press, 2000.
- [14] ANSYS, Inc., CFX – Solver Theory Guide Release 14.5, 2012.
- [15] Grawunder, M, Reiß, R, Stein, V, Breitsamter, C and Adams N A. Flow Simulation of a Five Bladed Rotor Head. *New Results in Numerical and Experimental Fluid Mechanics IX, NNFM*, Vol. 124, 2010, pp. 235-243.

Copyright Statement

The authors confirm that they, and/or their company or organization, hold copyright on all of the original material included in this paper. The authors also confirm that they have obtained permission, from the copyright holder of any third party material included in this paper, to publish it as part of their paper. The authors confirm that they give permission, or have obtained permission from the copyright holder of this paper, for the publication and distribution of this paper as part of the ICAS 2014 proceedings or as individual off-prints from the proceedings.